Enhanced adsorption–photocatalytic degradation of organic pollutants via ZIF-67 derived Co-N co-doped carbon matrix catalyst

Zheng Yang (✉ yang_chem@126.com)
China University of Mining and Technology

Heng-Shen Xie
Jiangsu Vocational Institute of Architectural Technology

Wei-Yuan Lin
Jiangsu Vocational Institute of Architectural Technology

Xian-Yong Wei
China University of Mining and Technology

Research Article

Abstract

A stable and efficient photocatalytic degradation of organic pollutants has been achieved *via* ZIF-67 derived Co-embedded N-doped nanoporous carbon materials catalyst (Co-N/C). The catalyst features well-distributed structures, suitable specific surface areas, and more active sites according to the various characterization analysis. Photocatalytic activity of Co-N/C was evaluated by the degradation of target pollutant Rhodamine B (RhB). As a result, the RhB could establish adsorption-desorption equilibrium in dark within 30 min and thoroughly degraded into H_2O and CO_2 by Co-N/C under a 500 W visible light irradiation in 40 min. Moreover, radical quenching experiments and reactive oxygen species monitor were performed to further probe the plausible photodegradation mechanism of RhB. Co-N/C is also appropriate for other alternative dyes and antibiotics affording ideal removal efficiencies. After the reaction, the Co-N/C could be facile separated by an external magnetic field and reused for 8 reaction cycles without obvious deactivation of its photocatalytic properties. This work is expected to provide an instructive guideline for the design of efficient and recyclable composite photocatalysts derived from metal-organic framework for a broad range of environmental remediation.

1. Introduction

With the rapid development of the world industrialization, water pollutions are serious increasingly and creating significant problems to the microorganisms and human society [1, 2]. Organic dyes and heavy metal ions are considered as the most carcinogenic and toxicity pollutants in wastewater because they directly threaten the water source quality and damage the ecological balance [3–5]. For the past several decades,, many techniques have been widely proposed for treating the organic wastewater, such as carbon adsorption, advanced oxidation, membrane technology, biological decomposition [6–9]. Among these, adsorption method is currently recognized as a simple, economical and practical technology to adsorb and remove wastewater pollutants. However, the regeneration/low efficiency of some adsorbents and the complex composition of industrial wastewater are still a problem. Therefore, it is urgent demand to probe more advanced protocols combined with adsorption technique for eliminating organic pollutants (OPs) from waste water in both scientific and industrial fileds.

Photocatalytic has been an overwhelmingly utilization in removal of OPs from the wastewater owing to its high efficiency, low cost and no any secondary pollutions [10]. A survey of the literature shows that semiconductor photocatalysts, such as TiO_2, ZnO, CdS, and $g-C_3N_4$ [11–14], were efficiently developed for the OPs degradation, in which the main products are less toxic organic molecules and inorganic CO_2, H_2O (NO_3^-, PO_4^-), as well as halide ions [15]. Moreover, the few surface active sites, easy agglomeration, and low solar energy utilization efficiency for some inorganic catalysts restrict their large-scale practical applications. Significantly, photocorrosion is a typical disadvantage of photocatalysis, and semiconductor photocatalysts are usually unstable under the operating conditions. The catalysts corrosion caused by light illumination in aqueous media contributes to the migration of metal ions and the dissolution of the solid photocatalysts [16, 17]. Carbon matrix materials generally have high

conductivity and good chemical stability [18, 19]. Improving carbon-based materials for building the composite catalysts could effectively promote charge transfer and extend [20, 21]. Thus, the exploitation of appropriate photocatalytic materials with stable and high-performance to remove OPs in water has been attracting great attention.

Metal-organic frameworks (MOFs) are functional porous coordination polymer [22–25]. Due to the flexible and diverse fashions of assembled with metal ion centers and organic ligands, MOFs materials possess versatile tunable chemical and physical properties [26–30]. In particular, MOFs are prospective and vital sacrificial templates/precursors for manufacturing nanoporous and doped carbon materials [31, 32]. Noteworthily, the metal ions could be encapsulated in ligand-derived carbon layers without obvious agglomeration by carbonization of the MOFs precursors containing the metal centers [33–35]. The synergistic effect of carbon materials and metals could accelerate the reactions and inhibit electron-hole recombination [36, 37]. For instance, Guo and co-workers developed Co_3O_4/C material catalyst by calcining activated carbon-modified MOFs precursor for the decolorization of methylene blue (MB) under UV-visible light [38]. Park et al. prepared ZnO/C hybrids by carbonization of MOF-5 and the obtained composite materials exhibited photocatalytic degradation on Rhodamine B (RhB) [39]. Similarly, Xia et al. exploited N-doped ZnO nanoporous carbon composites derived from ZIF-8 for CO_2 uptake and MB removal from water [40, 41]. With these in mind, the development of a highly performance and excellent stability photocatalyst based on the MOFs-derived nanoporous carbon materials materials is strongly desired for the degradation of OPs in waste-water.

Herein, a Co-encapsulated N-doped nanoporous carbon material was synthesized by a facile strategy (devoted as Co-N/C). The efficient and recyclable Co-N/C was prepared through pyrolysis carbonization of ZIF-67 parent, and then the catalyst was applied to the degradation of OPs. The degradation efficiency of RhB reaches 97.6% in a short time using Co-N/C with high stability and reusability. In addition, our results showed that the prepared Co-N/C could achieve efficient degradations of dyes and antibiotic under visible light irradiation. We further examined the reusability and regeneration of Co-N/C for 8 times. A feasible photocatalytic mechanism of Co-N/C was discussed *via* radical quenching experiments and electron paramagnetic resonance (EPR) technique.

2. Experimental

2.1 Materials

RhB, MB, methyl orange (MO), tetracycline hydrochloride (TCHC), norfloxacin, isopropanol (IPA), 1,4-benzoquinone (BQ), and ethylenediaminetetraacetic acid disodium salt (EDTA-2Na) were purpased from Energy Chemical Industrial Inc., Shanghai, China and used as received, respectively. 2-Methylimidazole (98%) and cobalt nitrate ($Co(NO_3)_2·6H_2O$, > 99%) were purchased from Sinopharm Chemical Reagent Co., Ltd., Shanghai, China. Solvents ethanol and methanol were obtained from commercial sources and purified by distillation prior to use.

2.2 Catalyst preparation

ZIF-67 precursor was prepared with some modification according to a previous literature procedures [42]. To a 50 mL Schlenk tube under air atmosphere, $Co(NO_3)_2 \cdot 6H_2O$ (1.55 mmol), 2-methylimidazole (67 mmol), and ethanol (50 mL) were successively added, stirring at 50 °C for 4 h. Then, the resulting residue was purified by recrystallization washing with ethanol (3⊆25 mL) to afford the desired product as purple precipitates.

Co-N/C was obtained by carbonization of ZIF-67 parent. Typically, ZIF-67 (2.0 g) was carbonized at different set temperatures for 5 h, then annealed to preparing the Co nanoparticles catalyst, denoting as Co-N/C(T), where T indicates the ZIF-67 MOFs thermolysis temperature (T = 600, 700, and 800 °C).

2.3 Characterization techniques of materials

Element compositions were collected by an ESCA LAB MK-II X-ray photoelectron spectrometer (XPS, Al Kα radiation). Bruker AXS D8 ADVANCE diffractometer was used to characterize the powder X-ray diffraction (XRD) patterns (Cu Kα source, λ = 1.5406 Å). Microscopic images were investigated by the scanning electron microscope (SEM, Hitachi S-3700 N) and transmission electron microscopy (TEM, JEM-2100, 200 kV). Specific surface areas were determined *via* Micromeritics analyzer at 77 K using the Brunauer-Emmett-Teller (BET) method (Autosotrb-IQ2-MP-XR).

2.4 Pollutant adsorption and photocatalytic degradation

RhB was utilized as a model pollutant to probe the adsorption of ZIF-67 precursor and Co-N/C. The adsorption performance was evaluated by dispersing 20 mg of the material in 20 mL RhB (10 mg/L) solution with stirring in the dark at room temperature, until the adsorption and desorption equilibrium was achieved. About 3 mL aliquots was sampled at certain interval and the solid was removed by a filter membrane (0.45μm).

Removal efficiency (R) of RhB was calculated by **Eq. 1**:

$$R = \frac{C_0 - C_t}{C_0} \times 100\% \qquad (1)$$

where C_0 and C_t are the concentration of RhB at contact time of 0 and t, respectively.

The reaction kinetic study was investigated by the pseudo first-order model Eq. 2.

$$-\ln(C_t/C_0) = k \bullet t$$

2

where k is the apparent rate constant of equation.

The photocatalytic degradation performances of materials were performed by using RhB solution with a 500 W Xe lamp (λ > 420 nm). Typically, a certain amount of Co-N/C was added into 20 mL RhB solution (10 mg/L) and then stirred for 30 min in the darkness. Then, after irradiation for an appropriate time interval, fixed amounts of the reaction system were taken out from the reactor and filtered by 0.45 μm filter membrane for further analysis. In addition, the effects of the photocatalyst dosage (4, 8, 12, 16, and 20 mg), photocatalytic degradation time (8, 16, 24, 32, and 40 min), and target pollutants (RhB, MB, MO, and TC) on the photodegradation performance were thoroughly researched. And the concentration of RhB, MB, MO, and TC in the solutions could be determined *via* UV−vis spectroscopy, and the *R* of the target pollutants was calculated according to the Eq. 1.

To demonstrate the reactive species involved in the photocatalytic reaction, IPA (2 mL), EDTA-2Na (1.0 equiv), and BQ (1 equiv) were used in photocatalytic experiments. Co-N/C was recycled and washed with methanol thoroughly, and dried at 60°C for 12 h. The collected photocatalyst was used for the cycle experiment of RhB degradation in the same condition.

3. Results And Discussions

3.1 Characterization of prepared materials

Scanning electron microscope image (SEM) (Figs. 1a and 1b) clearly exhibits a polyhedral structure and morphology for the synthesized ZIF-67 with a well-defined crystal shape and smooth surface. More importantly, the slightly rougher surface and relatively smaller particles on the surface of the Co-N/C can be observed, manifesting the gradual carbonization of the ZIF-67 (zeolitic imidazolate framework) (Figs. 1c and 1d). During the themolysis procedure, most cobalt oxide species were reduced to Co^0 with the carbonization of 2-methylimidazole in ZIF-67 [43]. Interestingly, the N-doped carbon matrix materials presented a prominent property in embedding the Co species, resulting in the high dispersion characters without apparent agglomeration. The mapping image observations detected the homogeneous distribution of C, N, O, and Co elements on Co-N/C surface. In addition, the content of C, N, and Co are ca. 60.3 wt.%, 10.2 wt.%, and 17.3 wt.%, respectively, from the analysis with energy dispersive X-ray (Fig. S1).

TEM captures the whole characteristic of the final sample (Figs. 2a and 2b). It is obvious that some favourably dispersed black nanoparticles (diameter: ~ 35 nm) were located on the surface of Co-N/C. Figures 2c further exhibits a typical high-resolution TEM image for the edge of Co-N/C, where the Co nanoparticles are entirely encapsulated by carbon matrix. The measured lattice spacing were 0.211 and 0.338 nm, assigning to the (111) plane of meatal Co and the (002) plane of graphitic carbon, respectively (Fig. 2d). The selected area electron diffractionpattern (Fig. 2e) of the Co-N/C nanoparticle verifies its polycrystalline structure.

The XRD patterns of synthesized ZIF-67 and Co-N/C were illustrated in Fig. 3a. Apparently, the peak at about 26.0° observed corresponds to the (002) plane of carbon (graphitic carbon). Other characteristic diffraction peaks of the lattice planes from Co-N/C at 44.2° (111), 51.6° (200), and 76.0° (220),

respectively, attributed to the metal Co, manifesting that ZIF-67 precursor could convert into Co-based materials by pyrolysis at high temperature [43, 44].

As Fig. 3b presents, the distribution curve for Co-N/C shows a typical type IV adsorption and desorption isotherms with a hysteresis loop, suggesting the existence of micro/mesoporous structure. According to the BET method, the surface area of Co-N/C was calculated as 379.32 $m^2 g^{-1}$ (Table S3). The micro/mesoporous and higher specific surface area are in favour of exposing more active sites and improve the efficiency of adsorption-photocatalytic reaction [45].

High-resolution XPS spectra analysis confirms the coexistence of Co 2p, C 1s, N 1s, and O 1s in Co-N/C (Fig. 4a). In addition, the atomic density of C, N, and Co are ca. 75.93 at.%, 9.56 at.%, and 4.80 at.%, respectively (Table S1), which is coincide with the EDX consequence. As shown in Fig. 4b, the two high resolution peaks of Co 2p at 781.3 and 796.0 eV could be attributed to Co 2$p_{3/2}$ and Co 2$p_{1/2}$, respectively [46]. Obviously, the Co 2$p_{3/2}$ regions consisted of three contributions at 778.8, 780.2, and 781.9 eV which are metallic Co, Co^{2+}, and Co^{3+} (cobalt oxides) [47]. The Co^{2+} and Co^{3+} species could originate from the surface oxidation of metallic Co. Among carbon regions, 3 characteristic peaks appeared at 286.8, 285.7, and 284.7 eV that are corresponding to the C−O bonds, C = N/C−N (sp^2), and C−C (sp^2) bonds [48] (Fig. 4c), respectively. For high-resolution N 1s spectra in Fig. 4d, the sample displayed four typical types of nitrogen species, attributing to the pyridinic-N (398.4 eV), Co-N (399.1), pyrrolic-N (399.6 eV), and graphitic-N (401.2 eV) [49, 50], which further manifested that N atom was doped successfully. Previous studies show that N-doping influences the electronic/ chemical properties and accelerates the photochemical performances for carbon materials [51]. In addition, higher contents of pyridinic-N and/or pyrrolic-N in Co-N/C material promote the electron transfer efficiency [52].

3.2 RhB adsorption experiments

Absorption experiments for RhB were explored to determine the adsorption capacity of Co-N/C. Figure 5a displays the UV-Vis absorbance spectra of RhB under dark conditions by using Co-N/C. Obviously, Co-N/C showed comparatively superior adsorption capacity of RhB at the first 20 min, and an adsorption-desorption equilibrium was gradually achieved afterwards. Adsorption quantity of RhB only slightly increased with prolonging the reaction time from 30 (20.1%) to 100 min (26.0%). In addition, compared with the direct visible light irradiation, adsorption-photocatalysis possessed a more higher removal efficiency, which was ascribed to the larger specific surface area and special composition of the Co-N/C improved the photocatalytic effect (Fig. 5c).

3.3 Photocatalytic degradation of RhB with various materials

As summarized in Table 1, catalytic activities of various materials were probed for the photocatalytic degradation of RhB for 40 min. Apparently, ZIF-67 precursor afforded the lowest photocatalytic performance and exhibited the maximum adsorption capacity (in darkness 30 min), which was attributed

to the ultrahigh surface area (Table S2). Co-N/C derived from ZIF-67 showed good activity in this photocatalytic system, and Co-N/C carbonized at 600 °C presented excellent catalytic activity, affording 97.6% removal efficiency. However, the Co-N/C (700) material with the largest RhB adsorption did not obtain the desired removal efficiency. The result further indicats that specific surface areas and adsorption abilities are beneficial to RhB photodegradation but not a decisive factor in this system. As shown in Fig. S2, Co NPs crystallization aggregation and particle size were increased at higher calcination temperatures (700°C and 800°C). Small particle size could increase surface-active catalytic sites to some extend and then promote photocatalytic RhB degradation.

Table 1

Photocatalytic performance of various materials for the degradation of RhB

Catalyst	Removal efficiency (%)						
	-30 min	0 min	8 min	16 min	24 min	32 min	40 min
ZIF-67	25.8	25.8	26.2	26.7	27.4	27.6	28.6
Co-N/C (600)	20.1	20.1	48.1	62.7	76.9	92.0	97.6
Co-N/C (700)	18.3	18.3	42.3	50.9	58.3	63.7	65.2
Co-N/C (800)	14.3	14.3	38.7	46.6	53.4	58.6	62.5
Reaction conditions: RhB 10 mg/L (20 mL), material (20 mg), adsorption time (30 min), photocatalytic (0–40 min).							

3.4 Degradation of RhB under different conditions

Optimization of the photocatalytic reaction conditions was performed by taking Co-N/C and RhB as the model substrates. Obviously, RhB could not degrade within 40 min when no catalyst was added, indicating that the self-photolysis of RhB was negligible. Figure 6 summarizes the photodegradation results of RhB with different conditions after the adsorption equilibrium. The optimal of contact time for the photocatalytic degradation of RhB was investigated in a range from 0 to 40 min. After only 8 min, *ca.*48.1% RhB could be effectively removed. It turned out that the photocatalytic degradation reaction could proceed in a short time in the presence of Co-N/C. The removal of RhB can be intuitively determined by the color change of the reaction system. A maximum RhB removal efficiency attained around 97.6% for 40 min. In addition, we have further examined the impact of catalyst dosage on reaction activities. Specifically, the RhB removal efficiency substantially increased as the Co-N/C amount increases from 4 to 20 mg and became maximum efficiency. With further increasing the Co-N/C feed to 24 mg, the removale fficiency of RhB decreased, which could be ascribed to the limitations on mass transfer and/or the light shielding effect caused by the excessive catalysts [53].

3.5 Photocatalytic degradation of other organic pollutants

The universality and scope of the photocatalytic activities of the prepared Co-N/C were further probed by degrading other alternative organic pollutants (MB, MO, TCHC, and norfloxacin) under the similar conditions. As Fig. 7a shows, 13.8% and 17.9% of the initial MB and MO are degraded, respectively, in darkness within 30 min, which manifested that the self-degradation efficiency of dyes is still not sufficient, and the enhancement of the photoexcited catalyst is essential. Interestingly, after only 16 min under irradiation, *ca.* 62.7% RhB, 47.7% MB, and 36.9% MO could be effectively degraded. It further confirmed the high catalytic activities and strong light harvesting capacities of the photocatalyst. As presented in Fig. 7d, 97.6% of RhB was removed in the presence of Co-N/C and about 70.1% and 59.8% of MB and MO, respectively, were degraded at the irradiation time of 40 min (Fig. 7d). In addition, Fig. 7b studied the pseudo-first-order kinetic model of organic dyes photodegradation. Obviously, the degradation of RhB exhibited the steepest straight line with the largest slope value among three dyes by the linear fitting, indicates the fast photocatalytic degradation proceeds on the photocatalyst. The apparent rate constant k of kinetic equation was summarized in Fig. 7c. The highest k value is achieved on RhB ($0.5938 \ min^{-1}$), followed by MB ($0.0041 \ min^{-1}$) and MO ($0.0039 \ min^{-1}$).

Furthermore, TCHC and norfloxacin were also used as the target pollutants to demonstrate the selectivity of Co-N/C. As indicated in Fig. 8a, both of the 13.8% of the initial TCHC and 8.0% of the initial norfloxacin are degraded under a dark condition for 30 min in the presence of Co-N/C, indicating that TCHC is less stable than norfloxacin. After 120 min irradiation, the total removal efficiency of TCHC and norfloxacin were reached *ca.* 61.8% and 55.7% respectively. Meanwhile, the reaction kinetics for degradations of TCHC and norfloxacin over Co-N/C are studied and depicted in Fig. 8b. The result accords with the pseudo-first-order kinetics and the rate of which could be acquired from the slope of the reaction plot. As expected, photodegradation of TCHC achieved a higher k value of $0.0105 \ min^{-1}$ over Co-N/C system, which was almost 2.2 times higher than that of norfloxacin ($0.0049 \ min^{-1}$). The high removal rates of organic pollutants (RhB, MB, MO, TCHC and norfloxacin) demonstrated the availability of Co-N/C photocatalyst.

3.6 Plausible Reaction Pathway of RhB degradation

To understand the main mechanism of photocatalyst degradation of RhB, the effect of several reactive scavenger species to the photocatalytic properties was performed. Specifically, IPA, EDTA-2Na, and BQ were used as $\cdot OH$, h^+ and $\cdot O_2^-$ scavengers[54], respectively. As presented in Fig. 9a, RhB can be almost completely removed without the addition of any scavengers. Meanwhile, it was found that $\cdot OH$ radical is not the main active species and made minor contribution to the RhB removal efficiency, since the presence of IPA caused only a slight decrease. Noteworthily, the removal efficiency of RhB was reduced to 44.7% and 64.2%, after the introduction of radical scavengers EDTA-2Na and BQ, respectively, which further demonstated that $\cdot O_2^-$ and h^+ dominated the photocatalytic degradation process. In addition, the electron paramagnetic resonance technique monitored the oxygen vacancies (active specie) of Co-N/C, which could further facilitate the separation of photogenerated carriers (Figs. 9b and 9c). With the above experimental results, the plausible photocatalytic degradation mechanism of RhB with Co-N/C was put

forward (Fig. 9d). In presence of the visible-light, the photogenerated electrons are transfer to the adsorbed O_2 on the Co-N/C surface to produce $\cdot O_2^-$. Subsequently, the resulting $\cdot O_2^-$ and h^+ could further degrade RhB to form small molecule compound (CO_2 and H_2O).

3.7 Reusability of Co-N/C for the photocatalytic degradation of RhB

The recyclability and stability of Co-N/C photocatalyst was probed under the optimum conditions. Co-N/C could be recycled by an external magnet field during the reaction solution after the reaction due to its good magnetic properties. As Fig. 10 exhibits, the degradation efficiency presents no apparent decrease after 8 times recycles. More than 95% of RhB removal efficiency maintained in the whole recycling reactions, which suggested that the good photocatalytic performance of Co-N/C could maintain over a longer time period. Further more, the XRD pattern analysis exhibits that the peak intensity and position of Co-N/C remained almost no shift, indicating its outstanding structural stability in 8 reaction cycles (Fig. S2a). Transmission electron microscopic image of the reuse catalyst shows there was almost no severe agglomeration of the Co nanoparticles on the Co-N/C surface, which could be ascribed to the stabilized structure derived from ZIF-67 MOFs and the highly dispersed Co nanoparticles (Fig. S2b). The above results further demonstrated that the stability and potential application in industrial fields of the prepared Co-N/C photocatalyst.

4. Conclusion

In this work, Co-N co-doped nanoporous carbon materials (Co-N/C) are obtained *via* a facile carbonization method by using ZIF-67 as precursors. The outstanding adsorption-photocatalytic performance toward Co-N/C is ascribed to its suitable specific surface areas, well-distributed structures, and the efficient transportation of photogenerated carriers. Notably, Co-N/C featured excellent degradation rate for the RhB in 40 min of visible light irradiation. Radical quenching experiments and reactive oxygen species monitor confirmed that h^+ ($\cdot O_2^-$) and oxygen vacancies dominated the photocatalytic degradation process of RhB. Co-N/C was also available for degradation of other OPs such as MB, MO, TCHC and norfloxacin. Moreover, the catalyst shows good stability for 8 reaction cycles without obvious deactivation. This work provides a simple strategy for fabrication of the doped porous carbon materials for enhancing adsorption−photocatalytic degradation of contaminants in wastewater.

Declarations

Ethical Approval

Written informed consent for publication of this paper was obtained from the Jiangsu Vocational Institute of Architectural Technology and all authors.

Competing interests

Availability of data and materials

The datasets used and/or analyzed during the current study are available from the corresponding author on reasonable request.

References

1. H. Wang, L. Zhang, Z. Chen, J. Hu, S. Li, Z. Wang, J. Liu, X. Wang, Chem. Soc. Rev. **43**, 5234 (2014).
2. T. Jayaraman, A.P. Murthy, V. Elakkiya, S. Chandrasekaran, P. Nithyadharseni, Z. Khan, R.A. Senthil, R. Shanker, M. Raghavender, P. Kuppusami, J. Madhavan, M. Ashokkumar, J. Ind. Eng. Chem. **64**, 16 (2018).
3. S. Renou, J.G. Givaudan, S. Poulain, F. Dirassouyan, P. Moulin, J. Hazard. Mater. **150**, 468 (2008).
4. Y. Li, Z. Geng, S. Yang, Z. Wang, T. Chen, X. Yu, Q. Guo, H. Rong, T. Duan, W. Zhu, Chem. Eng. J. **364**, 139 (2019).
5. S. Zhang, B. Li, X. Wang, G.B. Zhao, Z. Lu, T. Wen, J. Chen, X. Wang, Chem. Eng. J. **390**, 124642 (2020).
6. V. Katheresan, J. Kansedo, S.Y. Lau, J. Environ. Chem. Eng. **6**, 4676 (2018).
7. Z. Kong, L. Li, Y. Xue, M. Yang, Y.Y. Li, J. Clean. Prod. **231**, 913 (2019).
8. W.L. Wang, Y.Z. Cai, H.Y. Hu, J. Chen, J. Wang, G. Xue, Q.Y. Wu, Chem. Eng. J. **359**, 168 (2019).
9. B.M. Jun, J. Heo, N. Taheri-Qazvini, C.M. Park, Y. Yoon, Ceram. Int. **46**, 2960 (2020).
10. T. Yang, J. Peng, Y. Zheng, X. He, Y. Hou, L. Wu, X. Fu, Appl. Catal. B: Environ. **221**, 223 (2018).

11. J. Schneider, M. Matsuoka, M. Takeuchi, J. Zhang, Y. Horiuchi, M. Anpo, D.W. Bahnemann, Chem. Rev. **114**, 9919 (2014).

12. W. Chang, C. Sun, X. Pang, H. Sheng, Y. Li, H. Ji, W. Song, C. Chen, W. Ma, J. Zhao, Angew. Chem. Int. Ed. **54**, 2052 (2015).

13. H. Yang, Z. Liu, K. Wang, S. Pu, S. Yang, L. Yang, Catal. Lett. **147**, 2581 (2017).

14. Q. Bi, X. Huang, Y. Dong, F. Huang, Catal. Lett. **150**, 1346 (2020).

15. M.N. Chong, B. Jin, C.W. Chow, C. Saint, Water Res. **44**, 2997 (2010).

16. Z. Sha, H.S. Chan, J. Wu, J. Hazard. Mater. **299**, 132 (2015).

17. H. Lin, P.A. Maggard, Inorg. Chem. **47**, 8044 (2008).

18. C. Gao, S. Chen, Y. Wang, J.W. Wang, X.S. Zheng, J.F. Zhu, L. Song, W.K. Zhang, Y.J. Xiong, Adv. Mater. **30**, 1704624 (2018).

19. X. Sun, N. Habibul, H. Du, Chin. J. Catal. **42**, 235 (2021).

20. C.B. Bie, H.G. Yu, B. Cheng, W. Ho, J.J. Fan, J.G. Yu, Adv. Mater. **33**, 2003521 (2021).

21. W. Peng, X.X. Yang, L.C. Mao, J.H. Jin, S.L. Yang, J.J. Zhang, G. Li, Chem. Eng. J. **407**, 127157 (2021).

22. H.R. Moon, D.W. Lim, M.P. Suh, Chem. Soc. Rev. **42**, 1807 (2013).

23. T.K. Kim, K.J. Lee, J.Y. Cheon, J.H. Lee, S.H. Joo, H.R. Moon, J. Am. Chem. Soc. **135**, 8940 (2013).

24. J.K. Sun, Q. Xu, Energy Environ. Sci. **7**, 2071 (2014).

25. J.D. Xiao, H.L. Jiang, Acc. Chem. Res. **52**, 356 (2019).

26. P. Hu, J.V. Morabito, C.K. Tsung, ACS Catal. **4**, 4409 (2014).

27. X.B. Xu, Z.C. Zhang, X. Wang, Adv. Mater. **27**, 5365 (2015).

28. H.A. Hamad, W.A. Sadik, M.M. El-latif, A.B. Kashyout, M.Y. Feteha, J. Environ. Sci. **43**, 26 (2016).

29. W. Zhan, L. Sun, X. Han, Nano-Micro. Lett. **11**, 1 (2019).

30. G. Cui, W. Liu, L. Wang, R. Wu, C. Bi, D. Zhang, Y. Fan, J. Solid State Chem. **304**, 122562 (2021).

31. W. Zhong, H. Liu, C. Bai, S. Liao, Y. Li, ACS Catal. **5**, 1850 (2015).

32. J. Li, W. Xia, J. Tang, H. Tan, J. Wang, Y. Kaneti, Y. Bando, T. Wang, J. He, Y. Yamauchi, Nanoscale Horiz. **4**, 1006 (2019).

33. Z. Chen, R. Wu, Y. Liu, Y. Ha, Y. Guo, D. Sun, M. Liu, F. Fang, Adv. Mater. **30**, 1802011 (2018).

34. Y. Xu, W. Tu, B. Zhang, S. Yin, Y. Huang, M. Kraft, R. Xu, Adv. Mater. **29**, 1605957 (2017).

35. H. Zhang, T. Wang, J. Wang, H. Liu, T. Dao, M. Li, G. Liu, X. Meng, K. Chang, L. Shi, T. Nagao, J. Ye, Adv. Mater. **28**, 3703 (2016).

36. M. Zhang, Q. Dai, H. Zheng, M. Chen, L. Dai, Adv. Mater. **30**, 1705431 (2018).

37. H. Tian, C. Zhang, P. Su, Z. Shen, H. Liu, G. Wang, S. Liu, J. Liu, J. Energy Chem. **40**, 137 (2020).

38. J. Guo, Y. Zhang, Y.C. He, J. Shan, Polyhedron **175**, 114215 (2020).

39. S.J. Yang, J.H. Im, T. Kim, K. Lee, C.R. Park, J. Hazard. Mater. **186**, 376 (2011).

40. Y. Xia, B. Chen, Y. Zhu, D. Kong, P. Gui, Carbon **95**, 113 (2015).

41. M.Z. Hussain, A. Schneemann, R.A. Fischer, Y. Zhu, Y. Xia, ACS Appl. Energ. Mater. **1**, 4695 (2018).

42. J. Qian, F. Sun, L. Qin, Mater. Lett. **82**, (2012) 220.

43. R. Das, P. Pachfule, R. Banerjee, P. Poddar, Nano. **4**, 591 (2012).

44. F. Zhang, C. Yuan, J. Zhu, J. Wang, X. Zhang, X. Lou, Adv. Funct. Mater. **23**, 3909 (2013).

45. T. Ouyang, K. Cheng, Y. Gao, S. Kong, K. Ye, G. Wang, D. Cao, J. Mater. Chem. A **4**, 9832 (2016).

46. D. Barreca, C. Massignan, S. Daolio, M. Fabrizio, C. Piccirillo, L. Armelao, E. Tondello, Chem. Mater. **13**, 588 (2001).

47. G. Collinge, Y.Z. Xiang, R. Barbosa, J.S. McEwen, N. Kruse, Surf. Sci. **648**, 74 (2016).

48. Z. Wang, S. Peng, Y. Hu, L. Li, T. Yan, G. Yang, D. Ji, M. Srinivasan, Z. Pan, S. Ramakrishna, J Mater. Chem. A **5**, 4949 (2017).

49. Y. Xue, J. Liu, H. Chen, R. Wang, D. Li, J. Qu, L. Dai, Angew. Chem. Int. Ed. **51**, 12124 (2012).

50. L. Chen, C. Xu, R. Du, Y. Mao, C. Xue, L. Chen, L. Qu, J. Zhang, T. Yi, J. Mater. Chem. A **3**, 5617 (2015).

51. S. Wang, B.Y. Guan, X.W. Lou, Energy Environ. Sci. **11**, 306 (2018).

52. X. Xie, D. Su, J. Zhang, S. Chen, A.K. Mondal, G. Wang, Nanoscale **7**, 3164 (2015).

53. T. Yang, J. Peng, Y. Zheng, X. He, Y. Hou, L.Wu, X. Fu, Appl. Catal. B: Environ. **221**, 223 (2018).

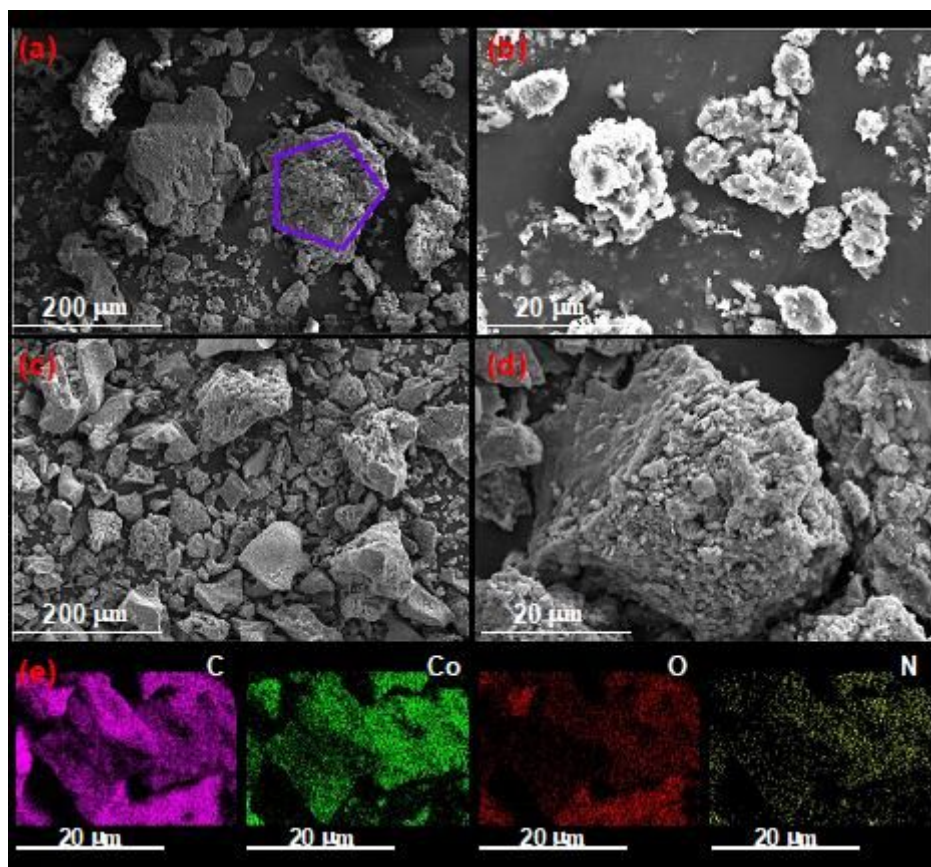54. Y. Nosaka, A.Y. Nosaka, Chem. Rev. **117**, 11302 (2017).

Figures

Figure 1

(a, b) SEM images of ZIF-67; (c, d) SEM images of Co-N/C; (e) the corresponding element mapping images of C, Co, O and N for Co-N/C.
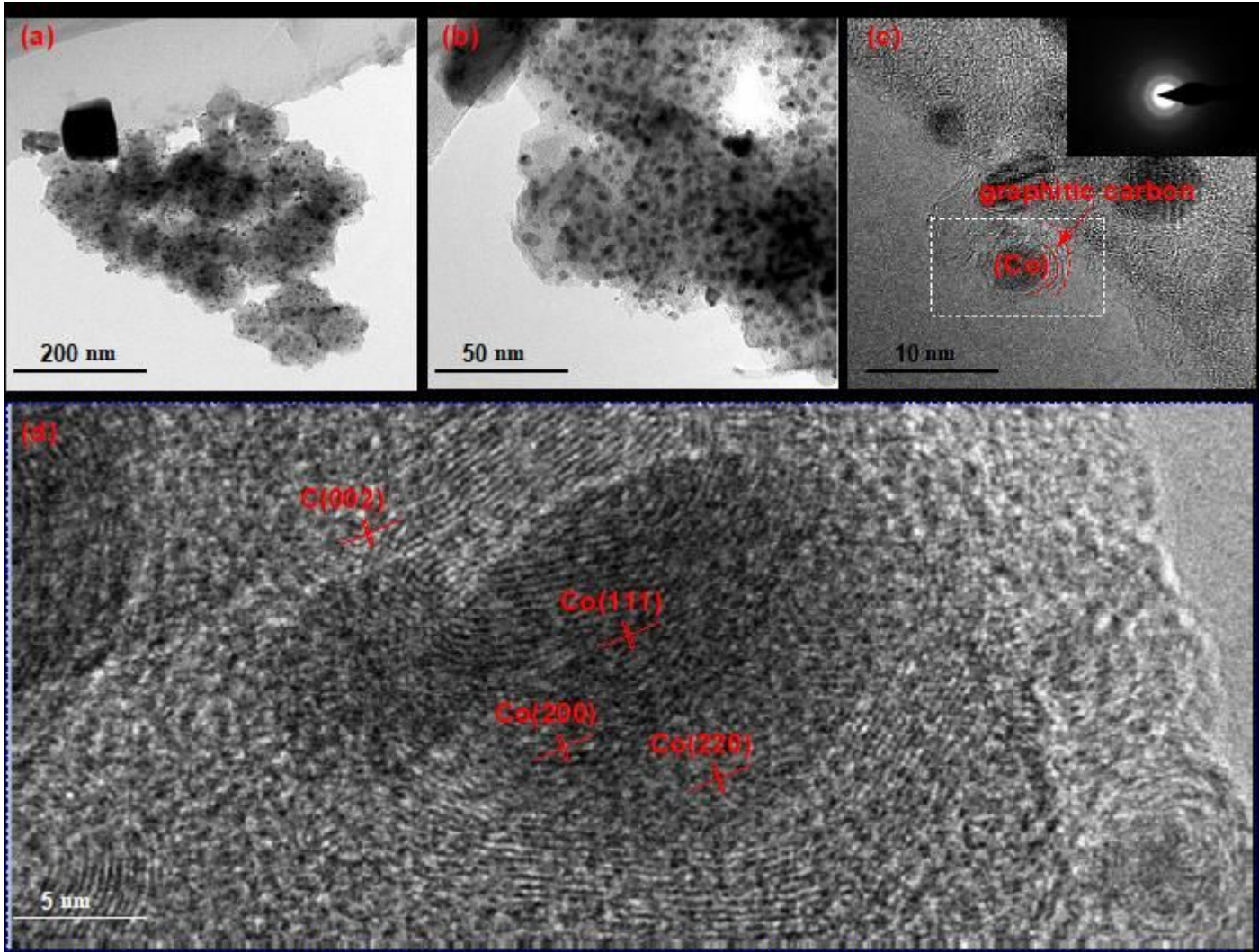

Figure 2

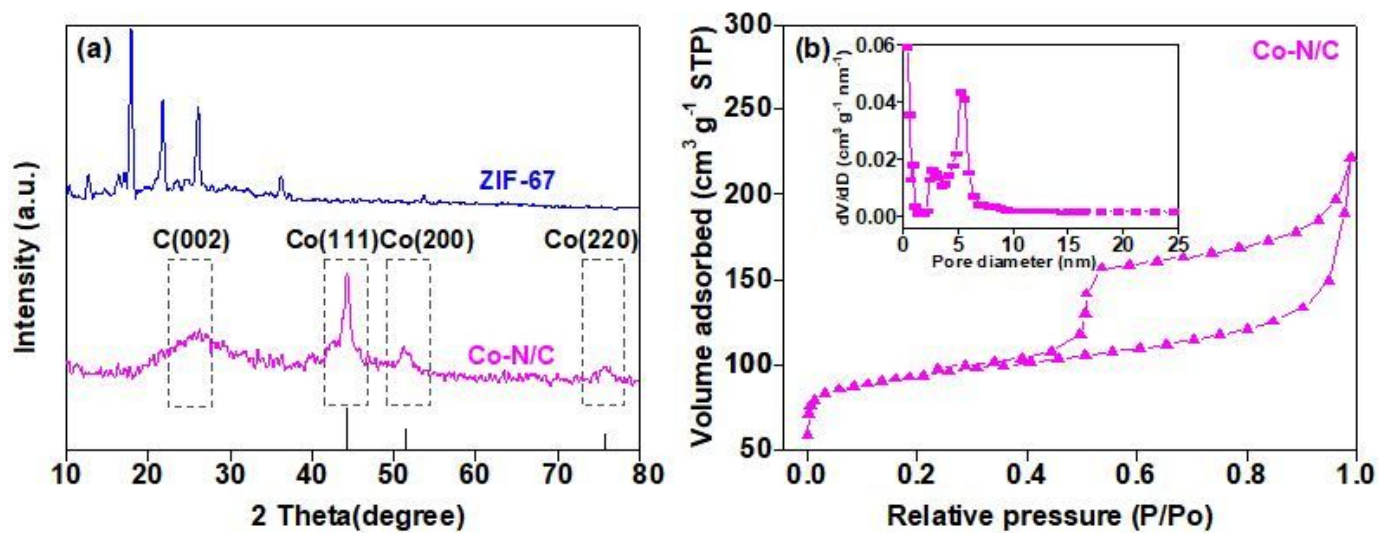(a, b,c) TEM images of Co-N/C; the inset image displays SEAD pattern of Co-N/C.

Figure 3

(a) XRD patterns of ZIF-67 and Co-N/C; (b) N_2 adsorption/desorption isotherms of Co-N/C, the inset image displays the pore size distribution curve.
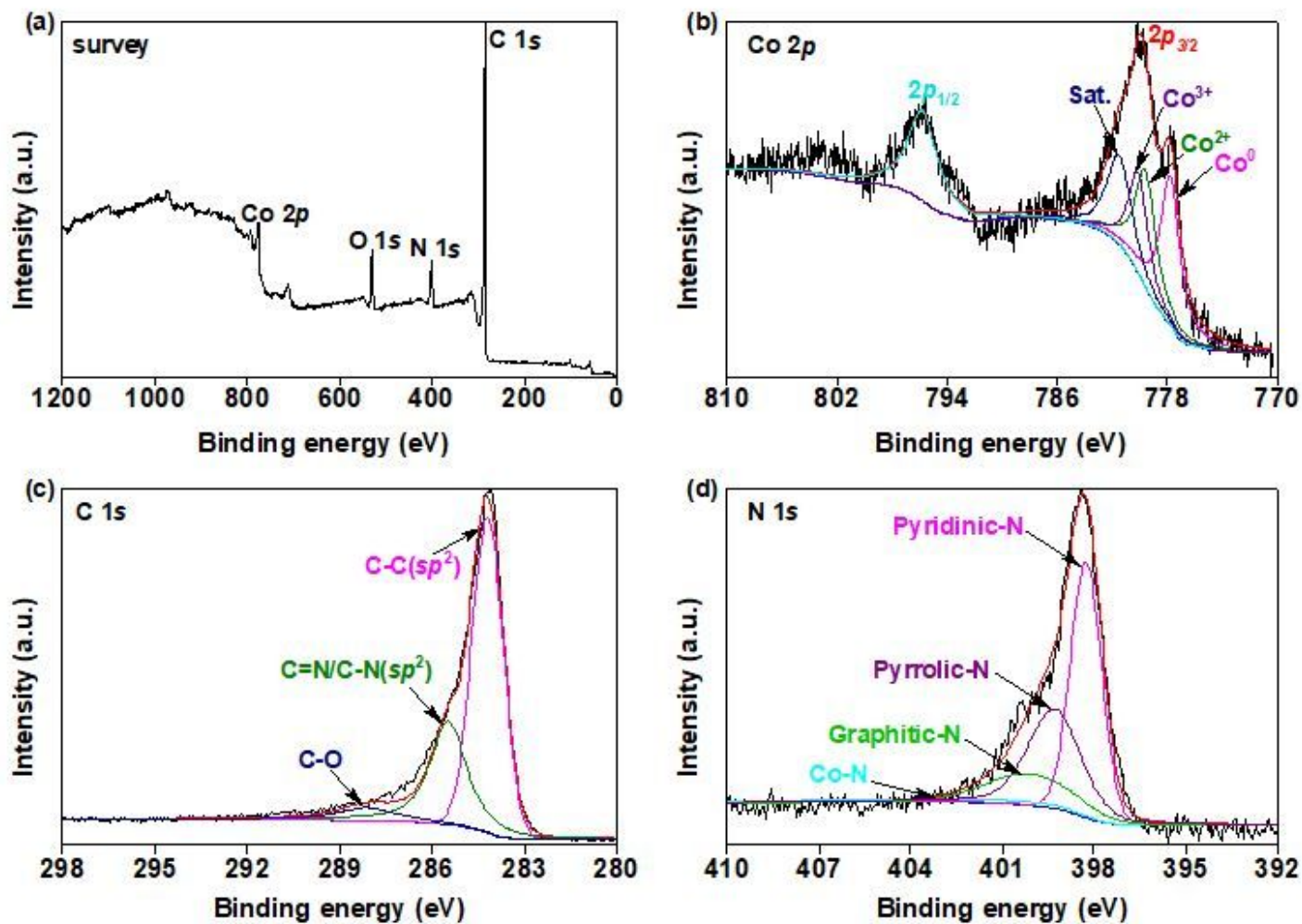
Figure 4

(a) The XPS of Co-N/C; (b) high-resolution Co 2*p* spectra of Co-N/C; (c) high-resolution C 1*s* spectra of Co-N/C; (d) high-resolution N 1*s* spectra of Co-N/C.
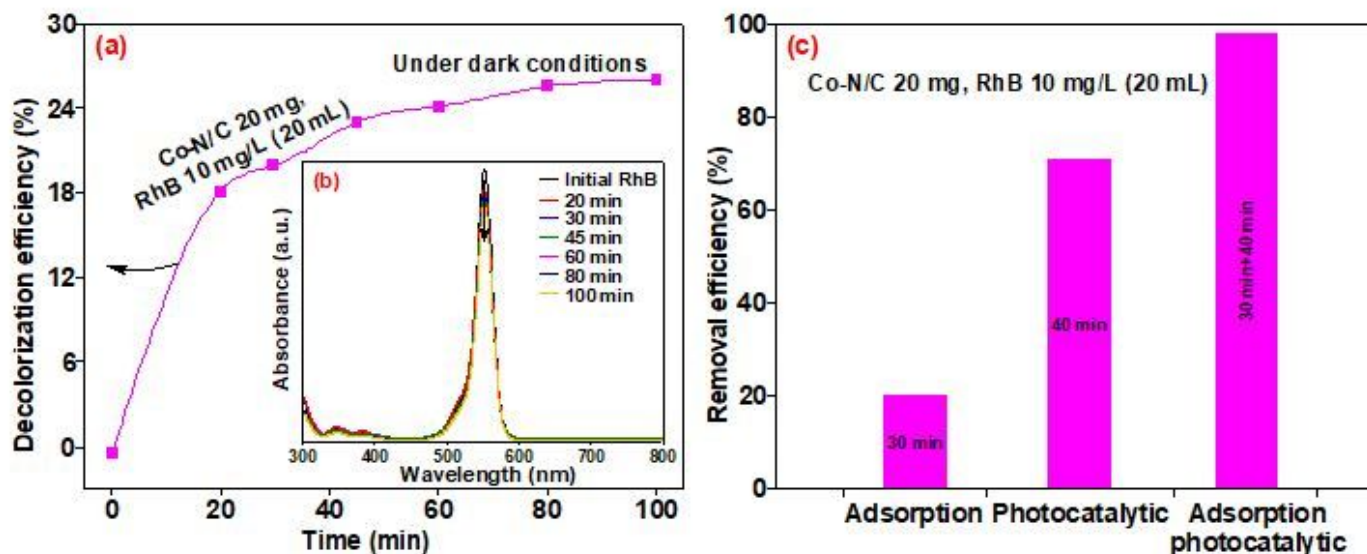
Figure 5

(a) Effect of contact time on RhB decolorization efficiency by Co-N/C in the dark. (b) Temporal UV−Vis absorption spectra of RhB in the presence of Co-N/C in the dark. (c) Removal efficiency of RhB over Co-N/C under different conditions.
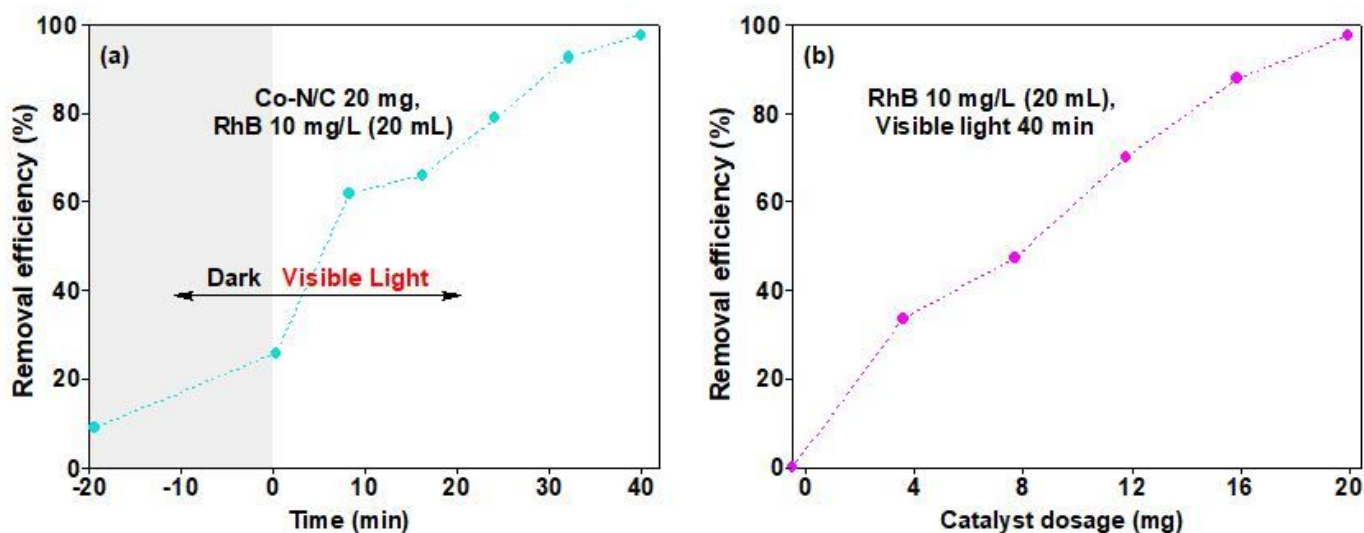
Figure 6

Effects of (a) contact time and (b) catalyst dosage on the RhB removal efficiency.
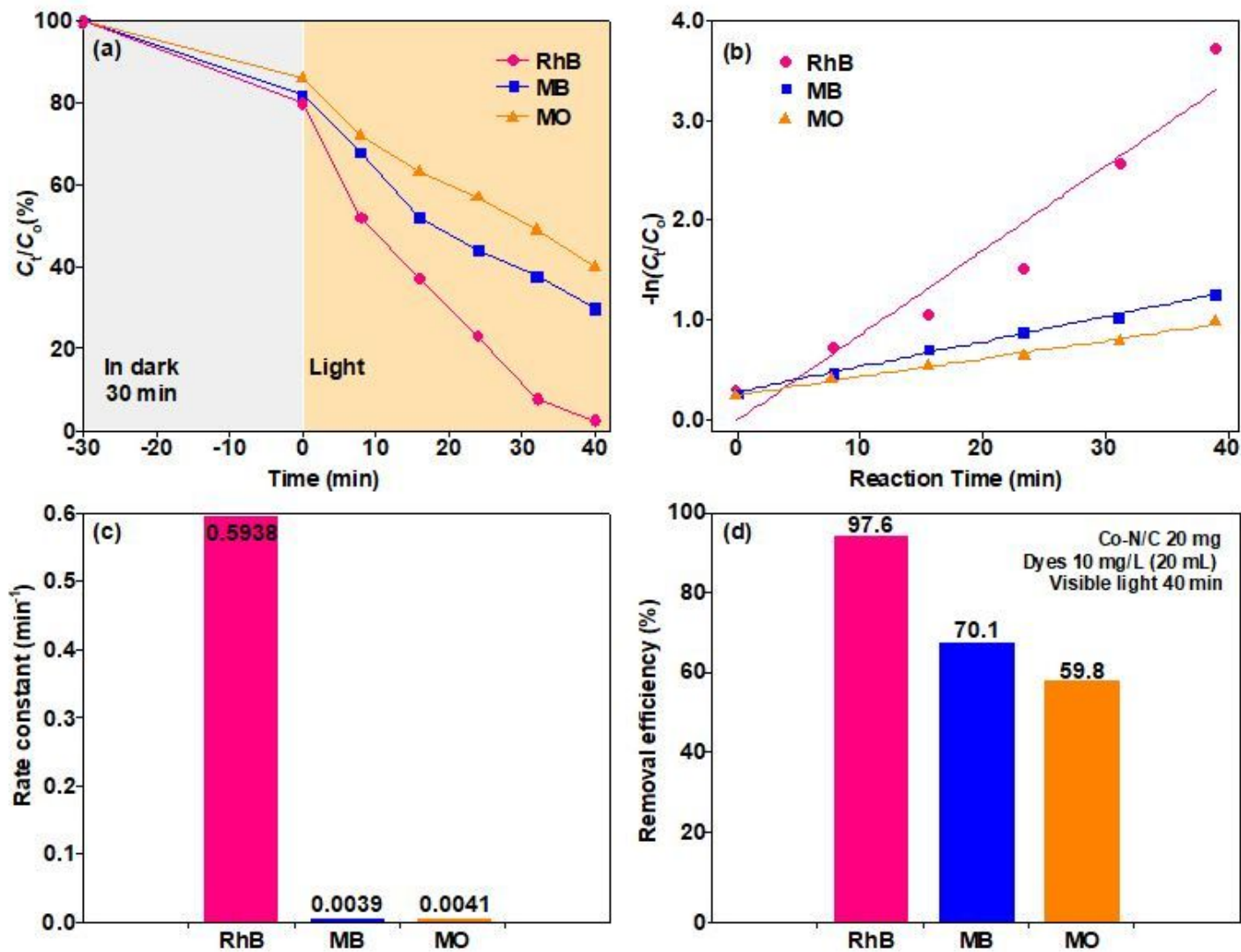
Figure 7

Photocatalytic degradation performances of Co-N/C: (a) total photocatalytic degradation curves of RhB, MB, and MO, (b) linear fitting of pseudo first-order kinetic equation, (c) the histogram of apparent rate constant, (d) effect of dye type on the removal efficiency under the same conditions.
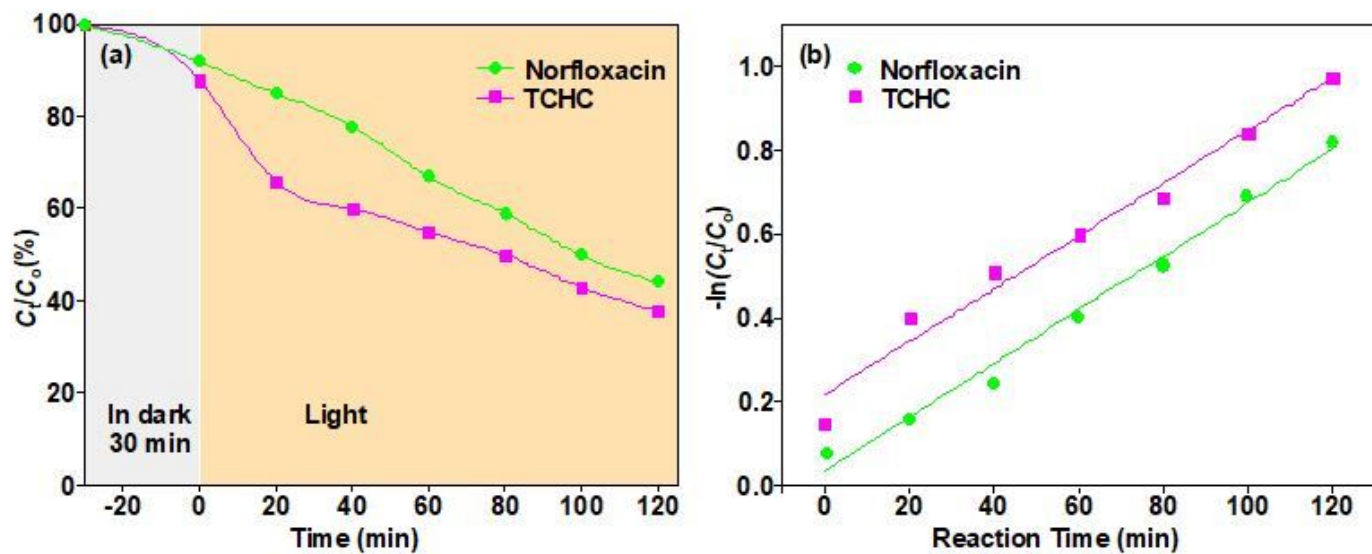
Figure 8

Photocatalytic degradation performances of Co-N/C: (a) total photocatalytic degradation curves of norfloxacin and TCHC, (b) linear fitting of pseudo first-order kinetic equation.
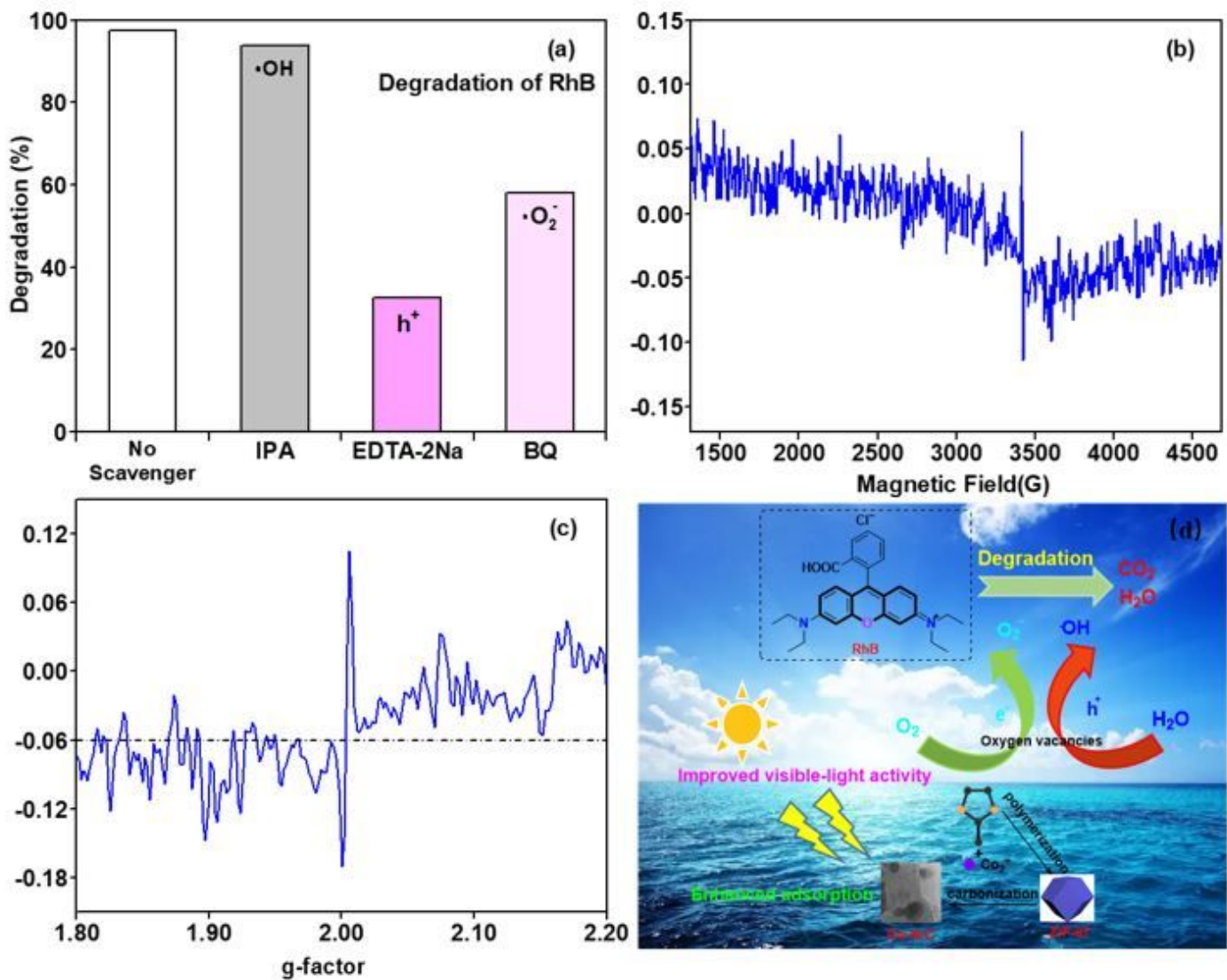
Figure 9

(a) Effect of different scavengers on the degradation of RhB over Co-N/C in water under visible light irradiation for 40 min; (b,c) the electron paramagnetic resonance Co-N/C; (d) plausible RhB photocatalytic degradation mechanism with Co-N/C under visible light irradiation.
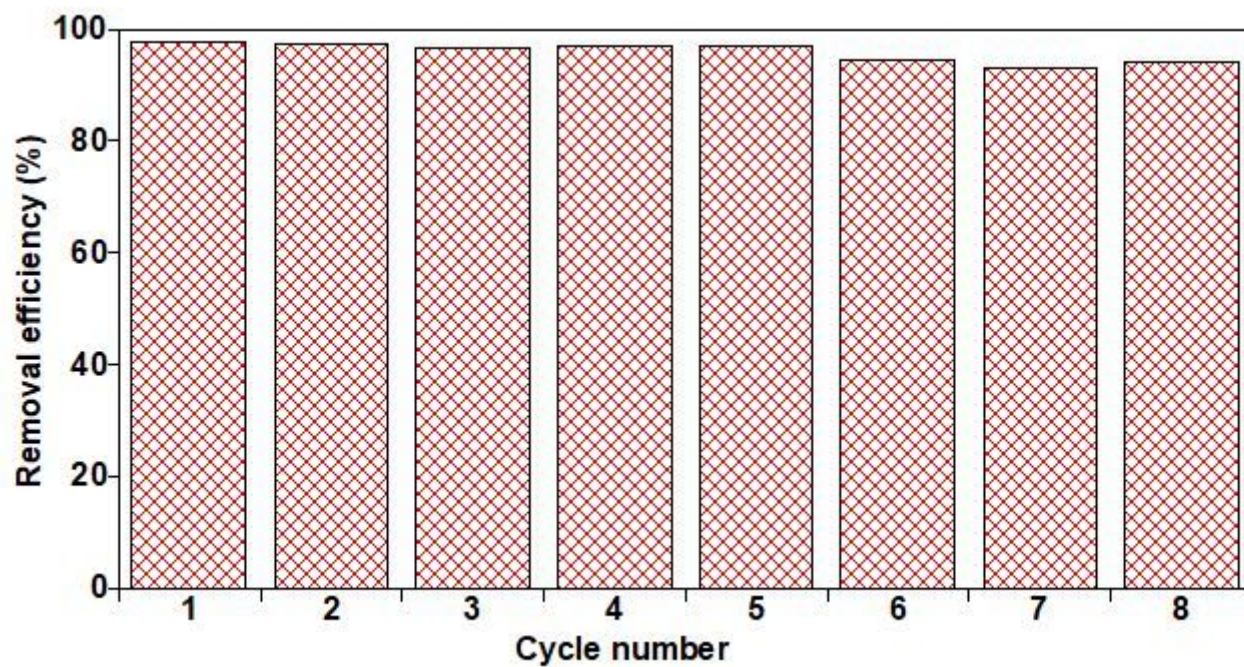
Figure 10

The RhB concentration changes in 8 reaction cycles under Co-N/C (initial concentration of RhB = 10 mg/L, irradiation time = 40 min).

Supplementary Files

This is a list of supplementary files associated with this preprint. Click to download.

- SI.docx